8

OPTICAL PROPERTIES

CARLA M. B. GONÇALVES, JOÃO A. P. COUTINHO, AND ISABEL M. MARRUCHO

8.1 INTRODUCTION

Polylactides (PLAs) have been known for several decades but only recently have these polymers gained commercial significance as a leading environmentally benign plastic available from renewable resources. Therefore, it is highly desirable to understand the optical properties of these materials so that they can be manipulated to develop materials of desirable characteristics for a specific objective. Optical properties such as color, clarity, and refractive index are important in dyeing operations for textile and in various packaging applications [1, 2]. Many of the physical properties of PLA are influenced by the amount and distribution of the *R*- and *S*-lactic acid stereocenters in the polymer chain, which reflect its history including the stereochemistry (*RR* (D-lactide), *SS* (L-lactide), *RS* (*meso*-lactide), or a mixture of equal amounts of D- and L-lactide referred to as racemic or DL-lactide) of the feed composition, polymerization kinetics, and extent of transesterification and racemization (see Chapters 1–4). As this rich variety of structures leads to materials with different characteristics, from fully amorphous to semicrystalline, a discussion on the PLA optical properties across a broad range of stereooptical compositions is valuable.

Since most applications of PLA-based materials are in the solid state, the detailed knowledge of the composition, bulk structure, and conformation of these materials is crucial. For example, it is well known that poly(L-lactide) (PLLA) obtained from LL-lactide is usually molded at 100–120°C in industrial melt processing because of the higher crystallization rate. It has been reported that when it is crystallized within this temperature region a mixture of crystals, α- and β-forms, is formed [2]. Although infrared and Raman spectroscopy is a very promising analytical technique, as will be shown below, many aspects of the optical properties for solid-state PLA remain unexplored.

In this chapter, the main optical techniques used to characterize PLA-based polymers are discussed in four sections: (1) absorption and transmission of UV–Vis radiation, (2) index of refraction, (3) specific optical rotation, and (4) infrared and Raman spectroscopy and NMR.

8.2 ABSORPTION AND TRANSMISSION OF UV–Vis RADIATION

Since the packaging industry, more precisely food packaging, plays a dominant role in the short term use of cheap nonbiodegradable petroleum-based materials, their replacement with PLA could provide a significant step toward a greener planet. In order to adequately preserve the quality of the food, the packaging materials have to provide efficient barriers against light, water vapor, atmospheric gases, and volatile organic compounds (VOCs), preventing food degradation and oxidation and preserving aromas and flavors [3]. The absorption and transmission of light by polymers is especially important in the food packaging industry where the packaged goods are light sensitive. Another issue in fresh food packaging is the effect of irradiation in the package since ultraviolet light irradiation is a common method used for lowering microbial population in foods [4].

Sensitive components of foods such as lipids, flavors, vitamins, and pigments may undergo degradation reactions when exposed to light. The spectrum and the intensity of the light source, the conditions of light exposure, and the degree of light transmittance of the packaging material are factors that can dramatically affect the food quality. Thus, packaging

Poly(lactic acid): Synthesis, Structures, Properties, Processing, and Applications, Edited by Rafael Auras, Loong-Tak Lim, Susan E. M. Selke, and Hideto Tsuji

plays a critical role in prevention of photodegradation of food components during storage. For example, it can slow down adverse reactions, namely, oxidation of fats and oils, formation of sensorially unpleasant volatile compounds (methional, aldehydes, and methyl ketones), loss of vitamins (riboflavin, β-carotene, and vitamin C), production or degradation of free amino acids, increase of the peroxide value, as well as discoloration of pigments, by absorption and reflection of the incident light [5, 6]. The design of the packaging for a specific food product involves not only the choice of the appropriate packaging material but also the addition of the right additives or stabilizers to the packaging in order to provide a more efficient UV–Vis light barrier, and thus a significant improvement in protected food quality after storage when compared to nonprotected food after storage, not to mention extended shelf lives.

The transmission of visible light (400–700 nm) and of ultraviolet radiation (100–400 nm) are important parameters in designing the right packaging to preserve and protect products until they reach the consumer. The photochemical degradation of plastics is mainly due to radiation known as UV-B (315–280 nm), because its high-energy content is capable of splitting certain chemical bonds [7]. Although this is an extremely important subject in food packaging applications, to our knowledge, only Auras [8] has measured the PLA visible and ultraviolet light barrier properties and compared them with the properties of commercial polymers traditionally used for food packaging. As can be seen in Figure 8.1 [7], at 225 nm PLA shows a significant increase in UV light transmitted when compared to other standard polymers, reaching about 85% at 250 nm and 95% at 300 nm. Thus, most of the UV-B and UV-A radiation passes through the films. No UV radiation transmission was found in the lower range of UV in 190–220 nm wavelength region. Within the group of conventional polymers, PS and cellophane transmit less radiation in the UV range where most foods are more sensitive and PET does not transmit any light in this wavelength range. LDPE is the polymer that shows the highest transmission of UV light followed by PLA [9].

When the subject of visible radiation is debated, its relationship with colors cannot be forgotten. Each wavelength in the visible light band causes a particular sensation of color. The human eye is not equally sensitive to light emitted at all wavelengths. It is most sensitive to the light in the yellow and green areas of the visible spectrum. When visible light of many frequencies strikes a surface of an object, this object will selectively absorb, reflect, or transmit certain frequencies, thus changing the color perception by the human eye. This selectivity is due to the fact that different atoms and molecules have different natural frequencies of vibration, and they will selectively absorb different frequencies of visible light. Reflection and transmission of incident radiation occur because the frequencies of those light waves do not match the natural frequencies of vibration of the objects. When radiation in these frequencies strikes an object, the electrons in the atoms of the object begin to vibrate. If the object is transparent, then the vibrations of the electrons are passed on to neighboring atoms through the bulk of the material and reemitted on the opposite side of the object. Such frequencies of light waves are said to be transmitted. If the object is opaque, then the vibrations of the electrons are not passed from atom to atom through the bulk of the material. Rather the electrons of atoms on the material's surface vibrate for short periods of time and then reemit the energy as a reflected light wave. Such frequencies of light are said to be reflected. Transparent materials are materials that allow one or more of the frequencies of visible light to be transmitted through them. Several important parameters are currently used to characterize visible light transmission and color of plastics, such as transparency (ASTM D1746-03

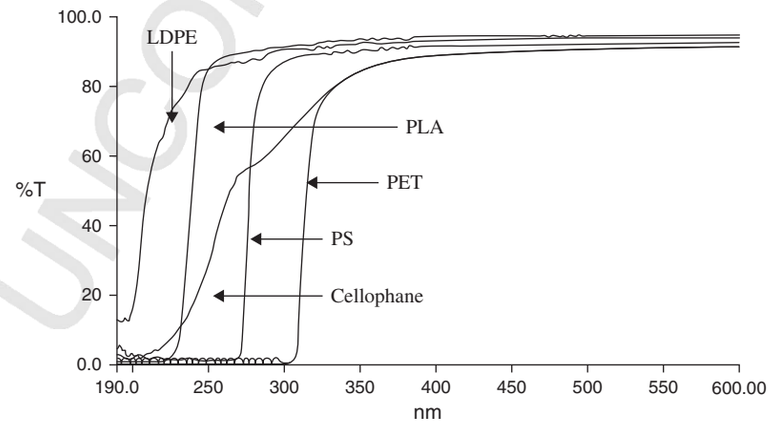

FIGURE 8.1 Percent transmission versus wavelength for PLA (98% L-lactide), PS, LDPE, PET, and cellophane films. Adapted from Ref. 7 with permission from Wiley-VCH Verlag GmbH & Co.

Standard Test Method for Transparency of Plastic Sheeting) and degree of yellowness (ASTM D6290-05 Standard Test Method for Color Determination of Plastic Pellets), which are based on the absorbance or transmission of UV–Vis light. The transparency, commonly known as "see through," is defined as the transmission of visible light in the 540–560 nm range [6]. The average transparency of food packaging films is around 95%. The degree of yellowness or the change in the degree of yellowness is a number calculated from spectrophotometric data that describes the change in color of a test sample from clear or white to yellow. PLA, PS, and LDPE have the same degree of yellowness, while cellophane and PET have higher values [7]. Since the light yellow color of PLA products could be a drawback in its application to the packaging industry, creating a consumer perception that the package is old, additives are usually used.

In particular, the development of color in PLLA when processed above its melting temperature is a limiting phenomenon in the production of PLLA-based products (implants, fabrics, textiles) by melt processing techniques, such as extrusion and injection molding. This problem adversely affects the properties and end use of the final product making it suitable only for low-grade materials or where color is not an issue. As a matter of fact, discoloration has been considered as one of the most critical problems that arises during melt processing of aromatic polyesters, including poly (ethylene terephthalate) [10, 11] and poly(trimethylene terephthalate) [12]. Wang et al. [13] successfully used UV–Vis spectroscopy for monitoring the process-induced degradation of PLLA during extrusion. UV–Vis spectroscopy provides a powerful and nondestructive tool for real-time detection of the thermal degradation of PLLA, which can be used to optimize the processing conditions since it is very sensitive to minute color changes of the PLLA melt. The observation of the spectra made possible the identification of a redshift of the absorption maximum of a polymer due to new chromophoric groups resulting from thermal degradation. It is known that the absorption maximum of a polymer is shifted to higher wavelengths when the number of conjugated double bonds increases [13, 14]. These authors concluded that pyrolytic elimination is the main degradation mechanism for dry PLLA, and is responsible for the color formation and molecular weight reduction; while an additional hydrolysis mechanism in moist PLLA only reduces molar mass but does not contribute to a change in UV–Vis absorption. A similar study was carried out by Gupta and Deshmukh [15] using PLA in a benzene solution by following the $n \rightarrow p^*$ transition characteristic of nondegraded PLA that occurs at 287 nm. Nevertheless, a blueshift of this absorption band occurs at 280 nm, suggesting that carbonyl carbon–oxygen bond cleavage is more efficient than other cleavages, which would result in the formation of –COOH groups on the polymer chain ends. Lalla and Chugh [16] dissolved PLA in chloroform and measured the maximum absorbance wavelength. They found this to be at 240 nm and attributed it to the ester group present in the polymer.

8.3 REFRACTIVE INDEX

Refractive index is a fundamental physical property of a substance that is often used for its identification, to confirm its purity or to measure its concentration. By definition, the refractive index of a medium is a measure of how much the speed of light is reduced inside the medium. It is a fundamental optical property of polymers that is directly related to other optical, electrical, and magnetic properties. Knowledge about this property is valuable due to its application in the design of new optical polymeric materials. The addition of nanosized inorganic or organic dopants to polymers allows the modification of the polymers' physical properties enabling the realization of functionalized polymers with new application fields, for example, in microoptics. For example, electron-rich organic dopants, dissolved in polymers, cause a pronounced increase in the refractive index.

Polymeric materials have refractive indices that depend on their structure. Lactic acid-based polymers can contain in their structure enantiomers of both L- and D-lactic acid. The most common structures have above 90% L-lactic acid enantiomers and are semicrystalline. Below this percentage, PLA becomes fully amorphous. Hutchinson et al. [1] studied the change in the index of refraction for PLAs by ellipsometric measurements. These authors did not find statistically significant differences in the refractive indices between samples of PLA with different enantiomeric compositions. Nevertheless, a decrease in the index of refraction (1.499–1.448) with the wavelength from 300 to 1300 nm was observed (Figure 8.2). This variation of index of refraction of PLA as a function of wavelength, λ (nm), can be described using the well-known Cauchy model given by Equation 8.1.

$$n(\lambda) = (1.445 \pm 0.00075) + \frac{4892 \pm 143}{\lambda^2} \qquad (8.1)$$

Also, many semiempirical group contribution methods derived from the refractive indices of liquid organic compounds as well as organic polymers have been established and give reliable predictions. These group contribution calculations are based on the molecular weight and molecular volume of the monomer, the density of the polymer, and the chemical structure of the polymer. The molar refraction values corresponding to group contribution models such as Lorentz–Lorenz, Gladstone–Dale, Vogel, and Looyenga have been collected extensively by VanKrevelen [17]. Auras et al. [7] reported PLA refractive indices calculated by Lorentz–Lorenz ($n = 1.482$), Gladstone–Dale ($n = 1.492$), and Vogel methods ($n = 1.482$).

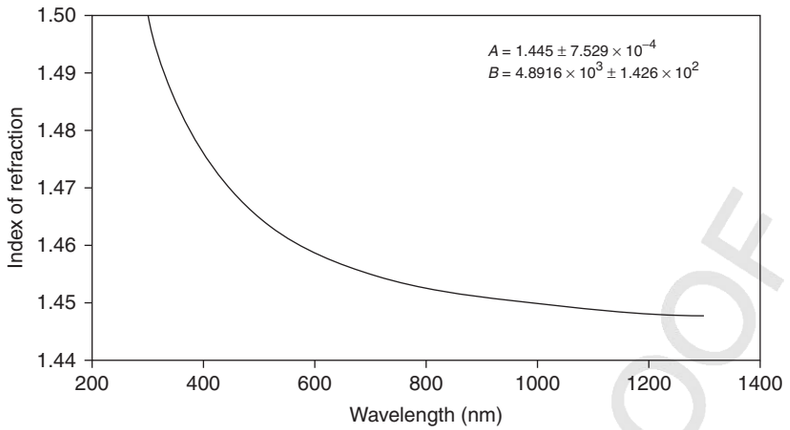

FIGURE 8.2 Index of refraction for PLA as a function of wavelength from a global determination of the Cauchy parameters across all optical compositions. Adapted from Ref. 1 with permission from American Chemical Society.

Malmgren et al. [18] determined the specific refractive index increment (dn/dc) for PLA with 16.4% of D-isomer, which is amorphous. The resulting dn versus concentration curve was measured using a differential refractometer. The authors gave two similar values for the resulting slope, dn/dc, 0.0237 ± 0.0034 and 0.0240 ± 0.0049 mL/g, since the experiments were very difficult to carry out due to air bubbles inside the sample. The obtained dn/dc values for PLA in chloroform are fairly small compared to those of other polymers such as polystyrene, which has a dn/dc of 0.169 mL/g in chloroform.

8.4 SPECIFIC OPTICAL ROTATION

The specific optical rotation of a pure material is an intrinsic property of that material at a given wavelength and temperature when dissolved in a particular solvent. The specific optical rotation [α] of PLLA and PDLA polymers was measured in chloroform at a concentration of 1 g/dL at 25°C using a polarimeter and wavelength of 589 nm. The values of α for PDLA and PLA were approximately $+150°$ and $-150°$, respectively [19–21]. Optical rotatory power along the c-axis of PLLA was found positive, while negative along the a-axis. This fact means that right-handed circularly polarized light propagates faster than left-handed circularly polarized light along the helix axis in PLLA. The reverse phenomenon takes place in PDLA. A gyration tensor component g_{33} of PLLA crystal along the c-axis was found to be extremely large, a few orders of magnitude larger than in the usual optically active crystals. Thus, the helical molecular conformations in helical polymers such as PLLA and PDLA produce huge optical activity. This phenomenon is important for the elucidation of gyro-optical properties of solids and promising for new optical applications utilizing their large optical activity [22].

8.5 INFRARED AND RAMAN SPECTROSCOPY

Infrared spectroscopy is a nondestructive analytical technique used to identify mainly organic materials. In general terms, the state of order of a macromolecular system can be defined by its constitution, configuration, conformation, regularity, stereoregularity, conformational regularity, and crystallinity. Vibrational spectroscopy of a polymer can give information about the state of order by analyzing different types of bands caused by different phenomena such as stereoregularity and conformational regularity of the polymer chain and the crystallinity of the polymer. While the conformational regularity depends on the intramolecular interactions between neighboring chemical groups of the same chain, the crystallinity depends on the intermolecular forces between adjacent chains. It is well known that vibrational spectroscopy is sensitive to local molecular environments, so differences can be observed between these two types of interactions. On the other hand, while these two properties, conformational regularity and crystallinity, are strongly influenced by the pretreatment of the polymer sample and the experimental conditions, the stereoregularity is only affected by chemical reactions [23].

IR and Raman spectroscopies are very important tools for characterization of the chemical and physical nature of polymers. Due to the high sensitivity of IR spectroscopy to changes in the dipole moment of a given vibrating group, this technique is intensively used to identify polar groups. In contrast, Raman spectroscopy is especially helpful in the characterization of the homonuclear polymer backbone due

its sensitivity to changes in polarizability [23]. The characterization of polymers using vibrational spectroscopy is based on empirical interpretation of IR or Raman spectra, since the bands are assigned to the independent vibration of atomic groups in the macromolecule and give information about the structural features of the polymer such as chemical composition, configuration, conformation, and crystallinity. However, a complete theoretical treatment in terms of the vibrational behavior of the polymeric system can only be obtained when the spectra data are obtained from isotope-substituted polymer analogues and polarization measurements on the specimens.

8.5.1 Infrared Spectroscopy

Early studies on PLLA mainly focused on the identification of characteristic bands to investigate the polymer crystallinity. Since Fourier transform infrared (FTIR) spectroscopy is sensitive to the conformation and local molecular environment, this technique has also been used to elucidate the structure of the crystalline polymers. More recently, research on PLLA surface characterization using FTIR has been an object of interest. This section is divided into three parts: structural analysis, surface characterization, and crystallization studies.

8.5.1.1 Structural Analysis: Band Assignment The FTIR spectrum of a polymer in the fingerprint region ($\nu \leq 1500$ cm^{-1}) is used to identify and characterize the material, since the observed peaks can be assigned to different vibration modes of chemical groups by comparison with cataloged FTIR spectra. Many authors [24–30] have used FTIR to characterize the structure of PLA-based materials (from new composite materials to polymer blends, to copolymers, to the effect of addition of plasticizers, just to mention a few) synthesized by different methods for different purposes and to establish differences in the obtained polymer at different experimental conditions. FTIR spectroscopy for measuring lactide concentration in a PLA matrix has been used by several authors who used different signals to normalize the characteristic lactide absorbance [31–34].

Several important articles have been published concerning the infrared and Raman spectra of PLA-based polymers. For example, one reference work is the pioneering study of Kister et al. [34] on the morphology, conformation, and configuration of PDLA and poly(*meso*-lactide) stereocopolymers using vibrational spectroscopy. Figure 8.3 shows the IR of the PLA polymers. PLAx is the acronym used to represent homopolymers and stereocopolymers, where x is the percentage of L-lactyl units. The differences observed in the several bands in the position, shape, or splitting clearly indicate that FTIR is a powerful technique to study PLA-based polymers.

In Figures 8.4 and 8.5, the attenuated total reflection FTIR (ATR-FTIR) spectra of semicrystalline $PDLA_{2:98}$ and amorphous $PDLA_{20:80}$ films are presented [36].

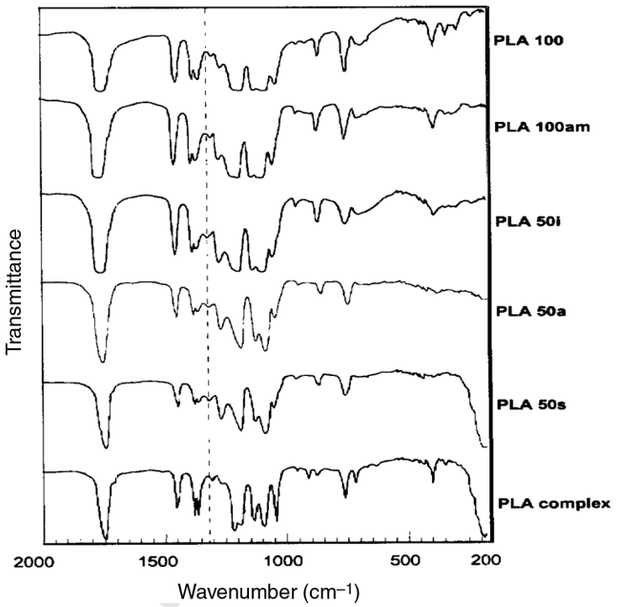

FIGURE 8.3 Infrared spectra of poly(L-lactic acid)s: PLA 100 (semicrystalline), PLA 100am (amorphous), PLA 50i (isotactic), PLA 50a (atactic), PLA 50s (syndiotactic), and PLA complex (stereocomplex). (- - -) Band sensitive to the tacticity. Adapted from Ref. 34 with permission from Elsevier.

The general band assignments for PLA-based polymers are presented in Table 8.1. The strong IR bands at 2997, 2946, and 2877 cm^{-1} are assigned to the CH stretching region ($-CH_{3(asym)}$, $CH_{3(sym)}$, and CH modes). The C=O stretching region appears in IR spectra at about 1759 cm^{-1} as a broad asymmetric band mainly due to A and E_1 active modes. The CH_3 is responsible for the appearance of the band at 1456 cm^{-1}. The CH deformation and asymmetric bands appear at 1382 and 1365 cm^{-1}. Moreover, the CH bending modes result in the bands at 1315 and 1300 cm^{-1}.

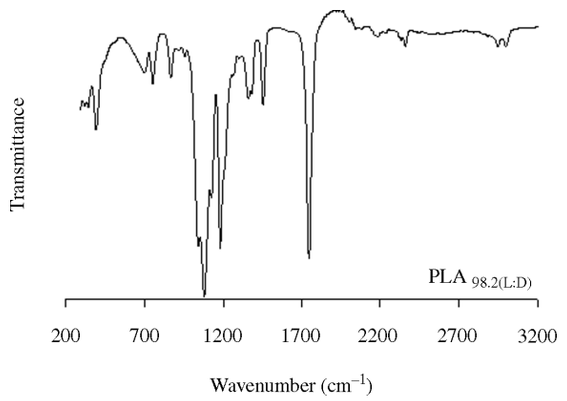

FIGURE 8.4 Infrared spectra of semicrystalline 98:2 (L:D)poly (lactic acid) [36].

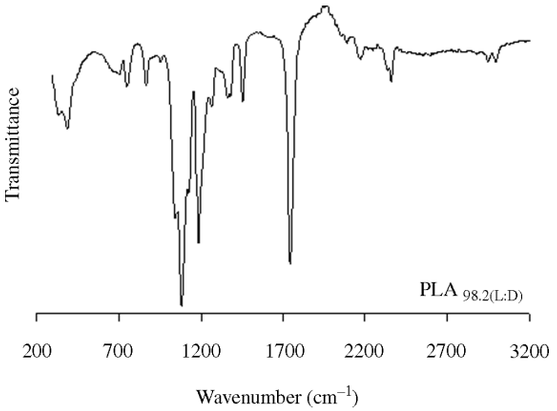

FIGURE 8.5 Infrared spectra of amorphous 80:20 (L:D)poly(lactic acid) [36].

The C–O stretching modes of the ester group appear at $1225\,cm^{-1}$ and the C–O–C asymmetric mode appears at $1090\,cm^{-1}$.

At 956 and 921 cm^{-1}, we can find the bands characteristic of the helical backbone vibrations with the CH_3 rocking modes.

At 871 and $756\,cm^{-1}$, appear two bands that can be attributed to the amorphous and crystalline phases of PLA, respectively. The bands that appear below $300\,cm^{-1}$ are mainly due to the CH_3 torsion modes and the skeletal C–C torsions [7, 34–37].

8.5.1.2 Surface Characterization Although transmission IR spectra contain information from both the bulk and the surface of the films, the majority of the signal arises from the bulk due to the much larger amount of polymer chains located there. However, a thorough knowledge of the surface structure of PLA is of great importance, since the surface constitutes a barrier to the surroundings and provides an adsorption site where chemical reactions can occur. A very suitable technique for surface studies of PLA is vibrational sum frequency generation (VSFG) spectroscopy. This is a nonlinear laser spectroscopy technique, which is inherently surface (and symmetry) sensitive under the electric dipole approximation for centrosymmetric systems.

A very interesting work on surface segregation and restructuring in PDLA and PLLA films of various thicknesses was presented by Paragkumar et al. [38] using ATR-FTIR. It was observed that PDLA surface segregation and the surface restructuring of methyl side groups are influenced by the polymer film thickness (e.g., poly(DL-lactide) films with thickness of 1 μm do not exhibit surface segregation of methyl side groups). On the other hand, poly(L-lactide) thin and clear films with thickness 15 μm undergo surface conformational changes upon solvent treatment with organic solvents such as toluene, acetone, tetrahydrofuran, and ethyl acetate. The solvent-treated surface of PLLA becomes hazy and milky white and its hydrophobicity increases compared to untreated surfaces. FTIR spectroscopic analysis indicated that polymer chains at the surface undergo certain conformational changes upon solvent treatment. These changes are identified as the restricted motions of C–O–C segments and more intense and specific vibrations of methyl side groups. Another study [39] using VSFG methodology in the CH stretching region demonstrated that this technique can generate valuable information to track changes in the surface and bulk structure of amorphous PLLA and PDLA films, and crystalline PLLA and PDLA:PLLA stereocomplex films. For crystalline PLLA, strong surface and bulk signals caused by both the order and the symmetry of the space group were observed. Amorphous PLLA and racemically composed PDLA were found to consist of a relatively disordered bulk.

VSFG spectroscopy has been widely and successfully employed to probe vibrational modes in the high-frequency region ($1500–4000\,cm^{-1}$) of the IR spectrum. However, these vibrations constitute highly localized modes. Therefore, such measurements mostly report on very local structural parts of the interfacial molecules (i.e., presence and orientation of $–CH_3$, –OH, and C=O groups). Recently, developments have been made to access a wider variety of surface chemical groups, such as the amide group that allows for the identification of α-helices and β-sheets (in molecules where amide bonds are present). This type of structural information still depends on the presence of a single chemical group. In contrast to high-frequency localized modes, low-frequency (skeletal) modes are often composed of the movement of several chemical groups. Thanks to their delocalized nature, these modes are extremely sensitive to the 3D structure of molecules.

Very recently, Sugiharto et al. [40] showed that knowledge of the structure of the first few monolayers of the PLLA/air surface of a biodegradable polymer can be achieved by performing femtosecond VSFG spectroscopy and that the bulk and the surface response appears through different order susceptibility elements. In its crystalline form, the backbone of a PLLA polymer is organized in a helical structure. The crystalline structure of PLLA has been determined to belong to the *P*212121 space group [41–43]. This particular combination of skeletal mode frequencies can be correlated to a helical structure in the polymer skeleton [43, 44].

The 3D surface structure of amorphous PLLA (L-A), crystalline PLLA (L-C), and racemic PDLLA (*R*) using femtosecond VSFG spectroscopy on delocalized modes in the fingerprint region for PLA was studied [45]. Figure 8.6 displays IR transmission spectra of the L-C, L-A, and *R* films. The IR spectra show some changes in the fingerprint region, which are characteristic of the three films.

Figure 8.7 displays VSFG spectra taken in the vibrational fingerprint region of the same films. The spectra of these three chemically identical films show a large diversity, in contrast

TABLE 8.1 Infrared Spectroscopy Data: Peak Band Assignments for Semicrystalline and Amorphous PLLA Infrared and Raman Spectra

IR $v(cm^{-1})$				Raman $v(cm^{-1})$				
Semicrystalline PLA	I	Amorphous PLA	I	Semicrystalline PLA	I	Amorphous PLA	I	Assignment
3571	w							νOH (free)
2997	M	2997	M	2995	S	2997	S	$\nu_{as}CH_3$
				2970	sh			$\nu_{as}CH_3$
				2960	sh			$\nu_{as}CH_3$
2947	M	2947	M	2943	VS	2942	VS	$\nu_{s}CH_3$
				2901	w			νCH
2882	w	2882	w	2877	M	2877	M	νCH
1760	VS	1760	VS	1773	S	1769	S	ν(C=O)
				1763	S	1755	sh	ν(C=O)
				1749	S			ν(C=O)
1452	S	1452	S	1452	S	1455	S	$\delta_{as}CH_3$
1348, 1388	S	1385	S	1384, 1388	M	1386	M	$\delta_{s}CH_3$
1368	S	1365	sh	1363, 1371	M	1365	M	$\delta 1$CH + $\delta_{s}CH_3$
1360	S	1360	S	1356	sh	1355	M	$\delta 1$CH + $\delta_{s}CH_3$
1300, 1313	M	1300, 1315	M	1293, 1302, 1315	S	1296, 1300	S	$\delta 2$CH
1270	S	1270	S			1264	sh	δCH + νCOC
1215	VS	1211	VS	1216	M	1216	M	ν_{as}COC
1185	VS	1185	VS	1179	M	1183	M	ν_{as}COC
1130	S	1130	S	1128	S	1128	S	$r_{as}CH_3$
1090	VS	1090	VS	1092	S	1092	S	ν_{s}COC
1045	S	1045	S	1042	S	1042	S	νC–CH_3
960	w	960	sh	954	Vw	953	sh	rCH_3 + νCC
925	w			923	M			rCH_3 + νCC
875	M	873	M	873	VS	873	VS	νC–COO
						790	w	γC=O
760	S	760	S	760	sh			δC=O
740	sh	740	sh	736	M	740	M	δC=O
715	M	710	M	711	M			γC=O
						700	Vw	γC=O
695	M	690	M	675	M	682	w	γC=O
				578	w	591	w	δ_1C–CH_3 + δCCO
515	w			520	M			δ_1C–CH_3 + δCCO
415	sh	415	sh	411	S	410	sh	δCCO
400	M	395	M	398	S	397	S	δCCO
350	M	345	M	347	w			δ_2C–CH_3 + δCOC
300	M	300	M	308	S	316	S	δ_oC–CH_3 + δCOC
295	sh	295	sh	300	w	300	S	COC deformation
				251	M	250	M	τCC
240	M	240	M	238	M	238	w	τCC
				208	M	194	w	τCC
				158	S	160	S	Skeletal torsion
				117	S	116	S	Skeletal torsion
				77	S	77	S	Skeletal torsion
				60	M			Skeletal torsion

The intensity, I, of each band is classified as VS (very strong), S (strong), M (medium), w (weak), sh (shoulder), s (symmetrical), and as (asymmetric) [7, 34–37].

to the IR spectra in Figure 8.6, which reflects the secondary and tertiary structure of the biopolymer at the interface. Such dramatic changes are not observed in Figure 8.6 because in linear spectroscopy, all atomic groups in the film participate in generating the signal so that it is the average bulk structure that is compared and not the interfacial one. Direct comparison between the VSFG spectra and the data in Figure 8.6 is therefore not very meaningful when it comes to determining

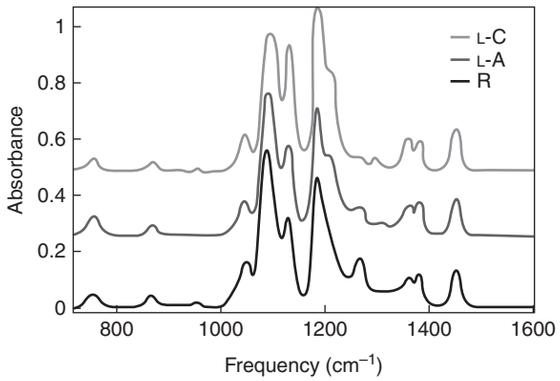

FIGURE 8.6 Infrared spectra of L-crystalline (L-C), L-amorphous (L-A), and racemic (*R*) PLA films. Since the materials are chemically identical, only small differences displaying the average bulk structure are observed. Adapted from Ref. 45 with permission from American Chemical Society.

the interfacial structure. Thus, VSFG experiments in the fingerprint region are extremely sensitive to changes in the backbone structure of the outermost polymer monolayer at the polymer/air surface. This previously largely unexplored frequency region allows the determination of whether the interfacial biopolymers are ordered helices (L-C interface), disordered helices (L-A interface), or rather consist of heterogeneously composed chains (*R* interface).

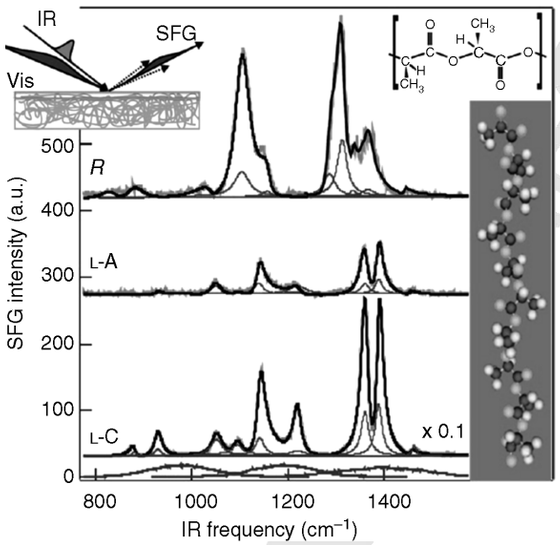

FIGURE 8.7 VSFG spectra of the delocalized modes of L-crystalline (L-C), L-amorphous (L-A), and racemic (*R*) PLA films, taken with three different IR pulses, which are displayed in the bottom. The black lines are fits to the data in which all contributions to the reflected electrical sum frequency field are added. The blue Lorentzians display the most prominent vibrational modes. The chemical repeat unit of L-PLA is also shown, as well as a molecular model of a 10_3 helix. In the top left panel, the VSFG experiment is illustrated. Adapted from Ref. 45 with permission from American Chemical Society.

8.5.1.3 Crystallization Studies It is well known that IR is sensitive to the local molecular environment. Accordingly, it has been widely used to explore variations in the intra- and intermolecular interactions and structural changes in macromolecules during melting, crystallization, and phase transition behavior of polymers. Generalized 2D correlation spectroscopy has been applied extensively to analyze IR spectra of polymers for three major reasons: first, it has powerful deconvolution ability for highly overlapped bands; second, it provides information about inter- and intramolecular interactions by correlating absorption band intensities of different functional groups; and third, the intensity changes of a specific sequence occurring during the measurement can be derived from the analysis of asynchronous spectra. In particular, the IR spectra of PLLA polymers are very sensitive to structural changes taking place during melt/crystallization.

Depending on the preparation conditions, three different crystalline modifications (α, β, γ) can be attained for PLLA. Recently, the fine details of dynamic processes during the crystallization of PLLA have become a matter of keen interest. The orthorhombic structure of the β-form, previously suggested from X-ray studies, was confirmed by trichroic vibrational analysis [43].

The structural evolution and crystallization dynamics of PLLA polymers during isothermal crystallization have been studied by IR spectroscopy. The two-dimensional (2D) correlation analysis of time-dependent IR spectra collected during the melt crystallization process revealed details about the intermolecular interaction of the CH_3 and C=O groups and the conformational changes in the C–O–C backbone that are not easily detected by conventional one-dimensional spectra. It was found that the intermolecular interaction of the CH_3 group appears during both the induction period and the growth period of PLLA melt crystallization, while the intermolecular coupling of the C=O group can only be observed during the crystallization period. The order formation of the C–O–C backbone during the induction period of PLLA melt crystallization can also be clearly observed in the 2D synchronous spectra. These observations show that the weak interchain interactions play an important role in controlling the nucleation and growth of polymer crystallization [2].

Detailed analysis of the three crystallization-sensitive regions is presented below.

(a) The C=0 stretching band region of 1860–1660 cm^{-1}. Despite extensive studies on the vibration spectra of PLLA α-crystal, the origin of spectral splitting is still not well interpreted, especially for the νC=O band. So far, it has been proposed that this splitting of νC=O band can be attributed to the intramolecular coupling [46] or correlation field splitting arising from

the interchain interactions, such as C–H···O hydrogen bonding [47, 48] or dipole–dipole [49]. Hydrogen bonding can be discarded from the analysis of the C–H stretching spectral region [43]. The intramolecular coupling is sensitive to the chain conformation and the distribution of conformers. The four components observed in the C=O stretching band of semicrystalline PLLA are attributed to the four possible conformers, gt, gg, tt, and tg, while in amorphous PLLA only bands corresponding to gt, gg, and tt conformers were found [46]. The correlation field splitting, also called factor group splitting or Davydov splitting, occurs due to the lateral interaction between the chains contained in the unit cell, splitting the absorption in a number of components. In the case of the orthorhombic unit cell of PLLA, the transition moments of the two adjacent PLLA chains can couple in phase or out of phase, leading to the splitting in the FTIR absorption [46].

(b) CH_3, CH bending and the C–O–C stretching band in the region of 1500–1000 cm^{-1}. Although in the range of 1500–1000 cm^{-1} the bands are highly overlapped, the band splittings of the CH_3 asymmetric deformation mode and C=O stretching during melt crystallization mode can be clearly observed in time-dependent IR spectra. It was found that the 1458 cm^{-1} band reflects the structural order of the CH_3 group, and the band at 1109 cm^{-1} is related to the C–O–C *trans*-conformation in the crystalline phase of PLLA. From 2D correlation analysis, it can be concluded that CH_3 groups form a close interchain contact during the induction period, causing the distortion of the 10_3 helix conformation of PLLA in α-crystals. On the other hand, the C=O groups of different PLLA chains do not come into close contact in the induction period [2].

The band at 1193 cm^{-1} is sensitive not only to the structural adjustment of the C–O–C backbone but also to the structural order of the CH_3 group in the crystalline phase. From the analysis of the difference spectra and 2D correlation spectra in the 1500–1000 cm^{-1} region, it is shown that the structural adjustment of the CH_3 group unambiguously precedes that of the ester group [49].

(c) The skeletal stretching and CH_3 rocking band region of 970–850 cm^{-1}. The absorption band at 921 cm^{-1} is found to be characteristic of the α-crystals and the 871 cm^{-1} band is sensitive to the 10_3 helix conformation. The former corresponds to a shorter critical sequence length than the latter. The bands at 955 and 860 cm^{-1} are proportional to the concentration of crystals in the α-form [2].

For polymorphic polymers, such as PLLA, the characteristic FTIR bands can be correlated to the different crystal modifications and typically stay distinguishable in a certain process. This makes it possible to illustrate the mechanism for a polymorphic transition process from the molecular level. It has been reported that when crystallized at this temperature region (100–120°C), a mixture of α′- and α-crystals is formed. Since the PLLA α′- and α-crystals show different FTIR spectra [50, 51], the structural changes during the annealing process could be detected by using FTIR spectroscopy.

The disordered crystal (α′-form) of PLLA was found to transform into the α-form during the annealing process at elevated temperatures. The α′ to α transition is very dependent on the annealing period (t_a: 0–1440 min) and annealing temperature (T_a: 120–160°C). With increasing T_a, the polymorphic transition progresses much more rapidly. As shown in Figure 8.8, the changes in FTIR spectra upon annealing are mainly associated with the splitting of νC=O and νC–CH_3 indicating that the α′ to α transition mainly involves the slight rearrangement of the chain conformation (especially related to the side groups) and packing manner in the unit cell to the more energy-favorable state, corresponding to the reduction of unit cell dimensions. It was proposed that the α′ to α transformation mainly proceeds by the direct solid–solid transition mechanism, since the direct solid–solid phase transition band (1500–1320 cm^{-1}) was observed during the annealing process. Moreover, it was found that M_w affects the crystalline phase transition significantly. In low molecular weight LLA samples, the α′ to α transition is much faster, and can proceed prominently even when annealed at relatively lower temperature [51, 52].

8.5.2 Raman Spectroscopy

The Raman spectra of PLA polymers are also characterized by a C=O stretching region. The C=O stretching mode in PLLA presents four active modes in the Raman region designated by A, B, E_1, and E_2, which could be observed at 1749, 1763, 1769, and 1773 cm^{-1}, as mentioned in Table 8.1. The PDLA Raman spectrum is characterized by broad and asymmetric lines. Two bands at 1769 and 1749 cm^{-1} appear in both PDLA and PDLLA stereocopolymer spectra. As this region of the spectra is very sensitive to changes in helical chain structure, any perturbation due to the introduction of (D,D) or (D,L) units causes the appearance or disappearance of these bands. Stereocomplexes can be identified by a sharp peak at 1745 cm^{-1} and a broad diffusion band at 1760–1780 cm^{-1}. This region proved to be very sensitive to the morphology and conformation. PLLA, PDLA, PLA complex, and poly(*meso*-lactic) stereocopolymers present CH_3 asymmetric deformation modes at about 1450 cm^{-1} in both IR and Raman spectra. Deconvolution analysis of the range between 1250 and 1400 cm^{-1} of the Raman spectra shows three groups of splitting bands at about 1390, 1360, and 1300 cm^{-1}, which are assigned, respectively, to the A, B,

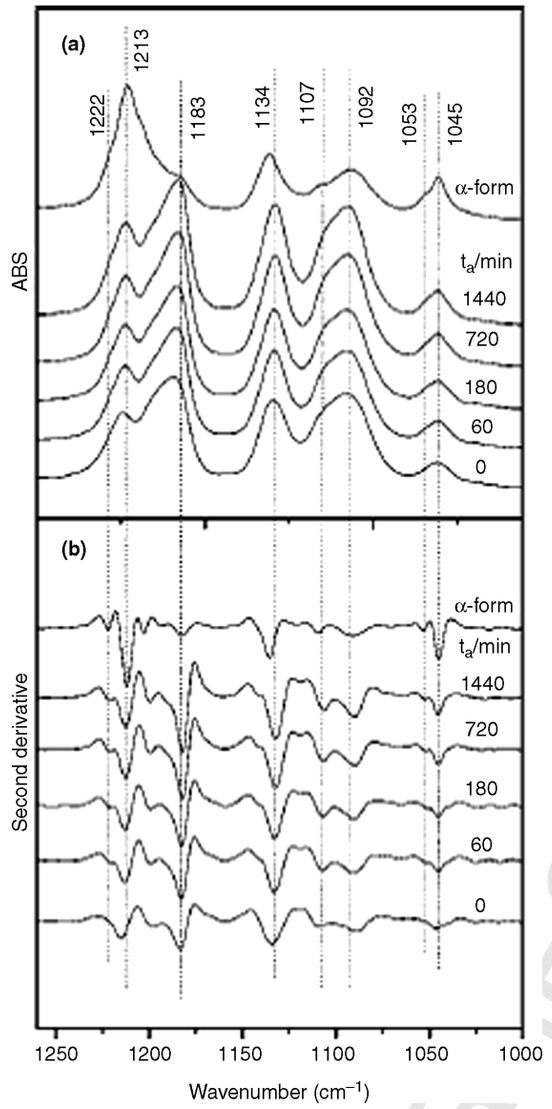

FIGURE 8.8 FTIR spectra (a) and corresponding second derivatives (b) in the frequency region 1260–1000 cm^{-1} recorded for the normal PLLA118 α-crystal and annealed (at 150°C for various periods (t_a/min)) PLLA118 α′-crystals. Adapted from Ref. 52 with permission from American Chemical Society.

E (E_1 and E_2) modes of the CH_3 and CH bending region [34]. Once again, it is possible to observe sharp and splitting peaks that characterize the semicrystalline PLAs, namely, PLLA and the PLA complex. As previously observed in the C=O stretching region, the amorphous state is characterized by asymmetric broad bands. For the (L,D)-PLA stereocopolymers, the bands at ∼1390 cm^{-1}, due to $\delta_s CH_3$ symmetric deformation, and ∼1300 cm^{-1}, due to δCH, are broad and with similar intensity and do not have significant shifts in the frequency. Next, we described the bands assigned to skeletal stretching and the rCH_3 rocking region, which appear between 1216 and 1179 cm^{-1}. Unlike the IR bands, the symmetric and asymmetric C–O–C modes of the PLLA present low-intensity bands in the Raman spectrum. At 1128 and 1042 cm^{-1}, two bands assigned to $r_{as}CH_3$ and νC–CH_3 stretching, respectively, can be found. The νC–COO stretching is responsible for the strong band at 873 cm^{-1}, which becomes broad and asymmetric for the (L,D)-PLA stereocopolymers and presents a shift to higher frequencies (880 cm^{-1}) for PLA complex. It is important to note the presence of a band at 920 cm^{-1} for the PLLA and at 908 cm^{-1} for the PLA complex (semicrystalline polymers), and the absence of any band near these frequencies in amorphous polymers (copolymers). The shifts in frequencies at which these bands appear for the semicrystalline polymers are mainly due to the different crystalline forms of each PLA. PLLA crystallizes preferably on left-handed helices while the crystalline PDLA (stereocomplex) adopts right-handed helices. Since the crystalline structure from the stereocomplex is racemic, the stereocomplex crystallizes in a triclinic unit cell to form a 3_1 helical conformation known as the β-form. In contrast, the individual polyenantiomers crystallize in a pseudo-orthorhombic system with two 10_3 helices, which is known as the α-form. The band at 920 cm^{-1} is assigned to α-forms while the other is due to β-forms [53]. Finally, in the low-frequency region, below 800 cm^{-1}, two bands, one of them in the range 736–760 cm^{-1} and the other in the range 650–677–711 cm^{-1}, are observed for PLLA. The corresponding bands of the PLA complex are sharp and located at slightly higher frequencies and correspond to δC=O and γC=O. The bands of the δCCO mode appear between 398 and 411 cm^{-1}. For the PLA complex, the δCOC skeletal chain deformation band appears in the range of frequencies (291–309 cm^{-1}) as a split line while bands characteristic of torsion modes are found at 239, 206, and 160 cm^{-1}. For PLLA, the associated bands are located at 230, 210, and 160 cm^{-1}. Raman spectra are more sensitive to modifications of chain morphology below 600 cm^{-1} [34, 35] as we can see in Figure 8.9.

Polarized Raman spectroscopy has been regarded as a powerful tool to quantify molecular orientation distributions, since it is capable of obtaining the fourth-order molecular orientation distribution coefficients, as well as the second order. This technique enables the molecular orientation distribution of the crystalline and the amorphous region to be determined independently. The PLLA Raman bands are assumed to be cylindrically symmetric owing to its helical molecular structure. A band at 926 cm^{-1} was assigned to the crystalline regions only of PLLA, whereas another band at 875 cm^{-1} was assigned to both crystalline and amorphous regions. The PLLA molecules were biaxially oriented in both amorphous and crystalline regions. The orientation distribution normal to the surface of the film was found to be broader in the amorphous regions than in the crystalline regions. Furthermore, a predominant unidirectional molecular orien-

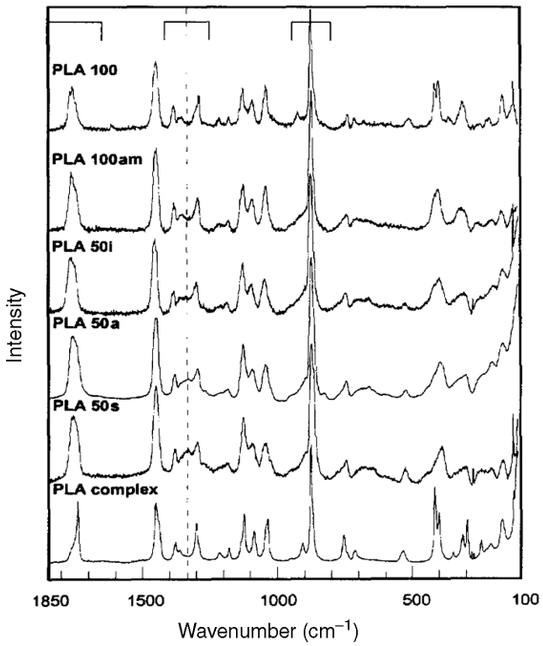

FIGURE 8.9 Raman spectra of poly(L-lactic acid)s: PLA 100 (semicrystalline), PLA 100am (amorphous), PLA 50i (isotactic), PLA 50a (atactic), PLA 50s (syndiotactic), and PLA complex (stereocomplex). (- - -) Band sensitive to the tacticity. Adapted from Ref. 34 with permission from Elsevier.

tation was observed in the crystalline region, whereas an isotropic molecular orientation distribution parallel to the surface was found for the amorphous phase [54] (Table 8.2).

Q1

Smith et al. [55] characterized using Raman the orientation of PLA films from NatureWorks used for food packaging and marketed by Cargill Dow Polymers. However, the study was carried out monitoring the changes in bands assigned to crystalline and amorphous phase as well as its orientation. The uniaxial and biaxial oriented films were characterized by Raman depolarization and Raman band shifts observed, respectively. Figure 8.10 shows a Raman spectrum of an unoriented film. The bands between 415 and 398 cm^{-1} should receive attention due to their relationship with the C–C–O bonds in the backbone. The band at 873 cm^{-1} can be assigned to a stretch of the C–C bond. There are two bands at 397 and 410 cm^{-1} with extreme sensitivity and selectivity to crystallization and orientation, which can be used to follow crystallization and to characterize orientation in the crystalline phase. The first band is assigned to the amorphous phase and the other is a crystalline band. When these films become oriented, these bands have marked shifts depending on the draw ratio, as can be seen in Figure 8.11 [55].

TABLE 8.2 Assignments for the FTIR Bands in the 1260–1000 cm^{-1} Region for PLLA α′- and α-Crystals [52]

IR Frequencies (cm^{-1})		
α′	α	Assignments
1213	1213	
	1222	ν_{as}(C–O–C) + r_{as}(CH_3)
1183	1183	
1134	1134	r_s(CH_3)
1092	1092	ν_s(C–O–C)
1107	1107	
1045	1045	
1053		ν(C–CH_3)

8.6 ^{1}H AND ^{13}C NMR SPECTROSCOPY

Nuclear magnetic resonance (NMR) spectroscopy has been used as a fundamental tool to understand the molecular structure of a wide variety of compounds. In polymer science, its applicability has proven to be extremely important for solid samples. The Zeeman interactions that happen between nuclei determine the average resonance frequency of a particular nuclear species, allowing the observation of specific elements without interferences of others present in the sample [56].

In the NMR spectra of PLA, the observed resonances can be assigned to stereosequence distribution in the polymer and reflect its history including the stereochemistry of the feed composition, polymerization kinetics, and extent of transesterification and racemization [57–60]. The assignments are designated as various combinations of "*i*" isotactic pairwise relationship (*RR* and *SS*) and "*s*" syndiotactic pairwise relationship (*RS* and *SR*). In the NMR spectra, the combinations *RR* and *SS* are indistinguishable and have identical chemical shifts, as would *RS* and *SR* [57, 61].

Zell et al. [61] assigned both the ^{1}H and ^{13}C NMR spectrum of the methine proton and carbon in PLA at the tetrad stereosequence level. They used a combination of two-dimensional NMR experiments and selective ^{13}C labeling and showed that the central pairwise relationship in the ^{1}H NMR spectrum is determined by the stereocenter in the lactic acid unit attached to the O terminus. They also determined that in the ^{13}C NMR spectrum the central pairwise relationship of the stereocenter in the lactic acid unit attached to the C terminus obtained consistent NMR and statistical data as can be seen in Figure 8.12. The chemical shifts of ^{13}C and ^{1}H nuclei in PLA are affected by the stereoconfiguration of two or three adjacent stereogenic centers on either side (hexad stereosensitivity) [62].

Kricheldorf et al. [59] proposed assignments for the stereosequences of the known microstructures of PLA, which were more recently confirmed by Zell et al. [61]. Figure 8.13 presents the ^{1}H and ^{13}C spectra of PLA synthesized using 5% L-lactic and 95% D-lactic obtained by Zell et al. [61].

In the ^{1}H NMR spectrum, the *sis* resonance, which appears at 5.24 ppm, gives an integrated intensity of 2.64%. Integration of the resonance at 69.21 ppm (the *isi*

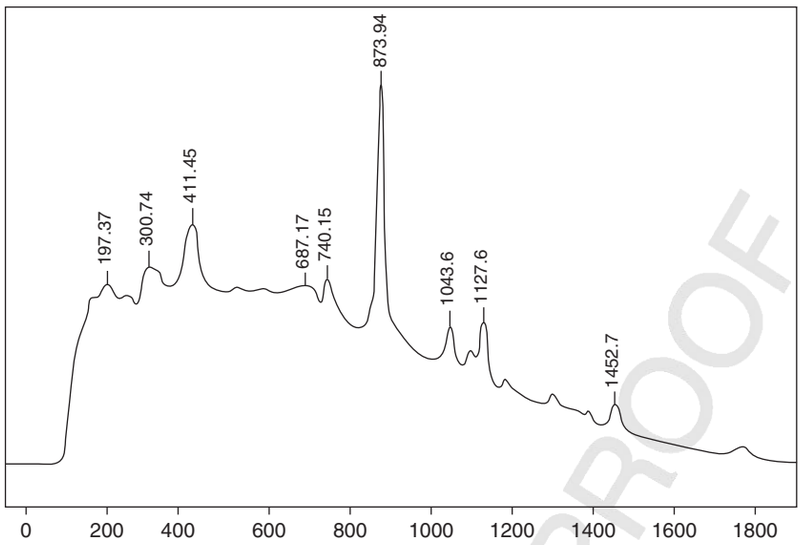

FIGURE 8.10 Raman spectrum of a 4.1% D-PLA unoriented cast film. Adapted from Ref. 55 with permission from John Wiley & Sons, Inc.

resonance) in the ^{13}C NMR spectrum gives a value of 6.19% [61]. When the PLA is synthesized using primarily D-lactide and small amounts of L-lactide that was ^{13}C labeled in the carbonyl position, only two peaks can be observed in the carbonyl region due to the ^{13}C labels, which confirms that almost all the pairs of *S* stereocenters are surrounded on either side by several *R* stereocenters [61]. The NMR spectra of PLA synthesized using (a) fully ^{13}C labeled and (c) unlabeled 5% L-lactide and 95% *meso*-lactide are shown in Figure 8.14, along with (b) the NMR spectrum of poly (*meso*-lactide). The spectra in Figure 8.14b and c are almost identical since the stereosequence distributions for 5% L-lactide/95% *meso*-lactide and for 100% *meso*-lactide are almost identical. The NMR spectrum in Figure 8.14a is very different from the spectra in Figure 8.14b and c. The reason is that the signals from the fully ^{13}C-labeled *S* stereocenters dominate the spectrum, which is similar to the situation observed in the one-dimensional ^{13}C NMR spectrum. As a result of the splitting of the signals for the ^{13}C-labeled *S* stereocenters into a doublet of doublets, the spectrum of the labeled polymer spans a larger chemical shift range (68.5–69.5 ppm) than the unlabeled polymer (69.0–69.4 ppm). The center of each set of doublet of doublets corresponds to the expected chemical shift value for

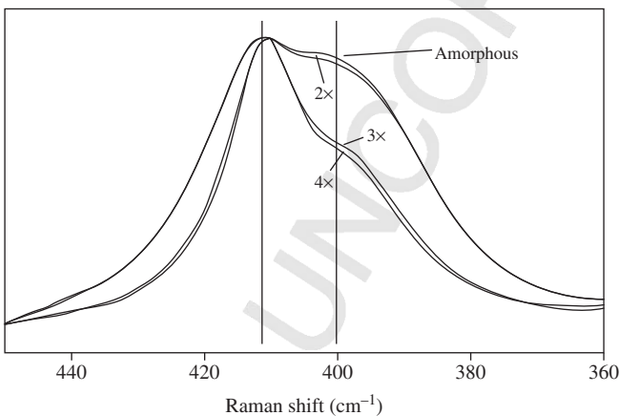

FIGURE 8.11 Raman spectrum of a 4.1% D-PLA-oriented cast film. Adapted from Ref. 55 with permission from John Wiley & Sons, Inc.

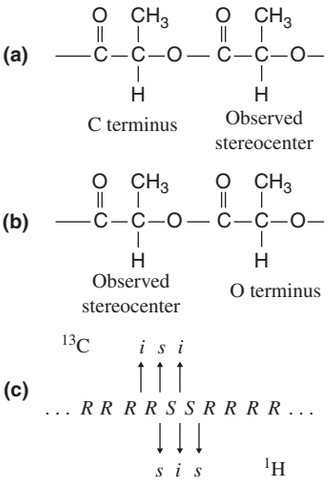

FIGURE 8.12 Diagram illustrating the alternative interpretation of ^{1}H and ^{13}C stereosequences: (a) central pairwise relationship determined by lactic acid connected to C terminus, (b) central pairwise relationship determined by lactic acid connected to O terminus, (c) direction of central pairwise relationship of ^{1}H and ^{13}C resonances. Adapted from Ref. 61 with permission from American Chemical Society.

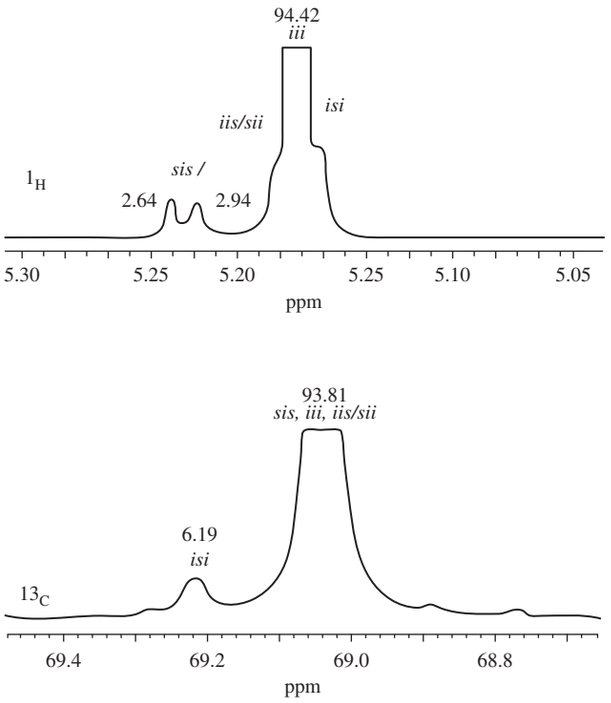

FIGURE 8.13 ^{1}H and ^{13}C solution NMR spectra of PLA synthesized using 5% L-lactide and 95% D-lactide. Adapted from Ref. 61 with permission from American Chemical Society.

an unlabeled carbon. The *sis* stereosequence is expected from both the unlabeled and labeled stereocenters. For the unlabeled *meso*-lactide component, an *isi* stereosequence is expected, while for the ^{13}C-labeled stereocenters, an *isi* stereosequence is not expected. In the unlabeled *meso*-lactide region, the *sis* resonance appears at 69.0 ppm and is not split, while in the ^{13}C-labeled L-lactide region, the *sis* resonance is centered at 69.0 ppm, but it is split into a doublet of doublets that extends ~0.4 ppm in both directions, spanning the region from 68.6 to 69.4 ppm. In addition, all of the other resonances expected due to the ^{13}C-labeled L-lactide lie within 0.1 ppm of the *sis* resonance, making the total span of all resonances due to ^{13}C-labeled L-lactide from 68.5 to 69.5 ppm (Figure 8.14). This experiment definitively proves that the peak at 69.0 ppm in the ^{13}C NMR spectrum is due to *sis*. If the *isi* and *sis* stereosequence assignments were reversed, then the *sis* peak would be centered at 69.2 ppm and would span from 68.8 to 69.6 ppm. The solid line in Figure 8.14 shows where the *sis* peak would be centered, the short-dashed line shows where the *iss*/*ssi* peak would be centered, and the two long-dashed lines show where the *isi* peak would be centered and where the farthest peak in that doublet of doublets should be. Since there is no resonance at 69.6 ppm, the assignment of the peak at 69.0 ppm to *sis* and the peak at 69.2 ppm to *isi* must be correct. It is also possible to definitively assign the *iss*/*ssi* stereosequences to specific resonances in the ^{13}C NMR spectrum. For a polymer that is synthesized with no isotopically labeled material, both the *iss* and *ssi* resonances will always have equal probability and therefore cannot be distinguished in the NMR spectrum. For PLA synthesized using 5% fully ^{13}C-labeled L-lactide and 95% *meso*-lactide, both the *ssi* and *iss* stereosequences are expected from the large amount of *meso*-lactide, and these resonances will not be split in the NMR spectrum. When PLA is synthesized using 5% fully ^{13}C-labeled L-lactide and 95% *meso*-lactide, only the *ssi* stereosequence will be split into a doublet of doublets because of ^{13}C–^{13}C*J* coupling to the methyl and carbonyl carbons. No peak due to *iss* will be observed from the ^{13}C-labeled stereocenters. If the *ssi* resonance is centered at 69.1 ppm, the doublet of doublets will overlap the doublet of doublets generated by the *iii*, *iis*, *sii*, and *sis* stereosequences, and the spectrum will span from about 68.7 to 69.5 ppm (Figure 8.6). If the *ssi* resonance occurs at 69.4 ppm, the doublet of doublets will span from 69 to 69.8 ppm. The ^{13}C NMR spectrum in Figure 8.14a has no resonance above 69.5 ppm, indicating that the resonance at 69.1 ppm in Figure 8.14b is due to *ssi*, while the resonance at 69.4 ppm is due to *iss* [61].

Thakur et al. [62] studied PLA samples with various compositions of L-lactide, D-lactide, and *meso*-lactide: sam-

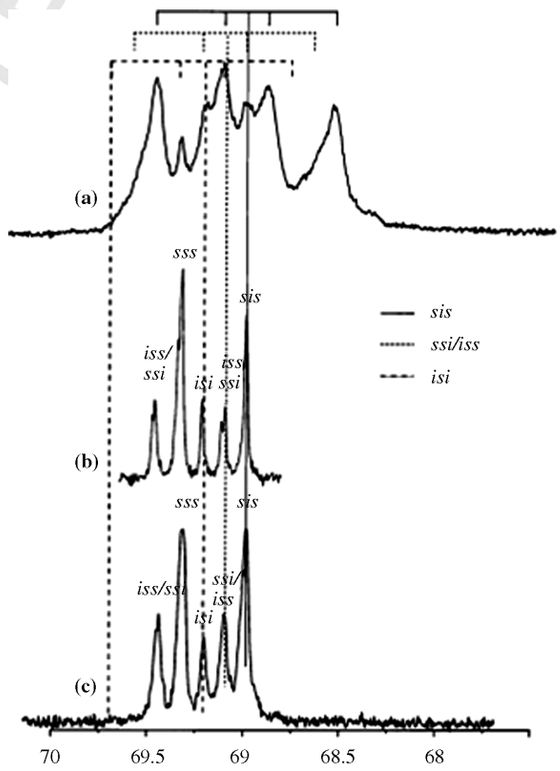

FIGURE 8.14 ^{13}C NMR spectra of PLA synthesized using (a) 5% fully ^{13}C-labeled L-lactide and 95% *meso*-lactide, (b) *meso*-lactide, and (c) 5% L-lactide and 95% *meso*-lactide. Adapted from Ref. 61 with permission from American Chemical Society.

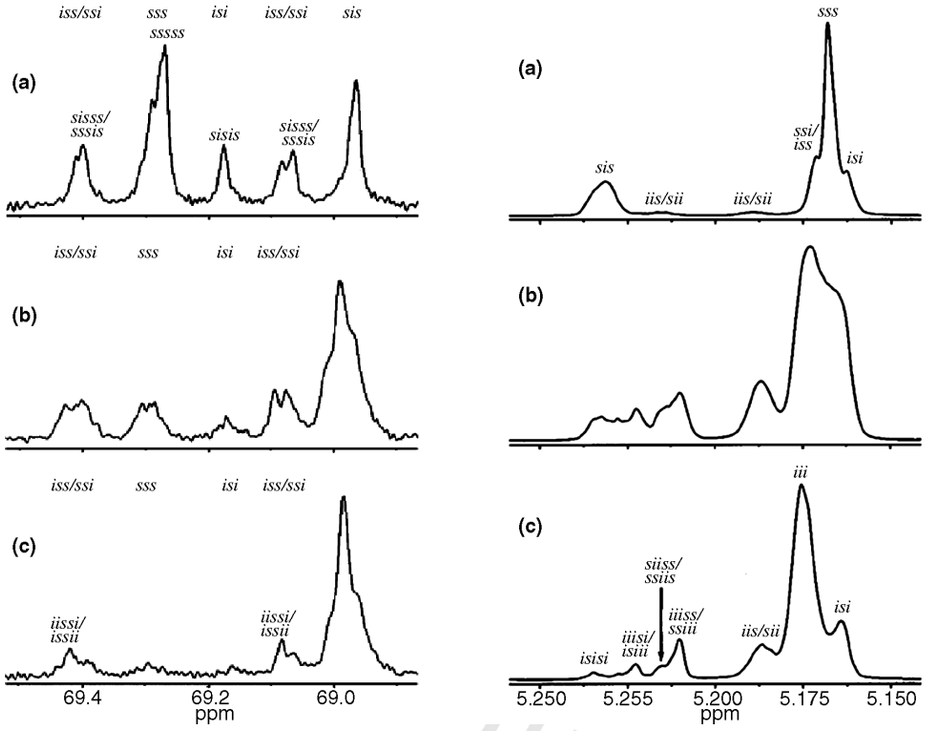

FIGURE 8.15 Left: methine resonances in the ^{13}C NMR spectra of poly(lactide) samples (a) 1, (b) 2, and (c) 3. The peak at about 68.95 ppm comprises resonances from *iii*, *iis*, *sii,* and *sis* core stereosequences. Right: methine resonances in the homonuclear decoupled ^{1}H NMR spectra of poly (lactide) samples (a) 1, (b) 2, and (c) 3. Adapted from Ref. 62 with permission from American Chemical Society.

ple 1 had 3% of both L-lactide and D-lactide and 94% of *meso*-lactide; sample 2 had 51.5% of L-lactide, 1.5% of D-lactide, and 47% of *meso*-lactide; and sample 3 had 70.9% L-lactide, 0.9% D-lactide, and 28.2% *meso*-lactide. They found that the carbonyl resonance in ^{13}C spectrum of PDLLA indicates a higher stereoselectivity than hexad and is most likely to be octad [62]. However, due to the high degree of overlap, the assignments of the peaks for octad stereosequences to carbonyl resonance and probably a hexad stereosensitivity to methyl resonance are difficult. Based on hexad stereosequences, the authors [62] interpreted the ^{13}C methine resonances and the stereosequences *sss*, *isi*, *ssi*, and *iss* are well resolved and their assignments are consistent with previous studies made by Kricheldorf [59], Schindler and Harper [63], or Kasperczyk [58].

Although ^{1}H NMR allows better results regarding stereosequence probabilities, there are still some questions regarding the coupling between the methyl protons and the methine (–CH) protons at each of the stereogenic centers in PLA.

As was observed by analysis of ^{13}C spectra, also in ^{1}H spectra the peaks corresponding to hexad stereosequences can be observed (Figure 8.15). The intensity distribution of the various stereosequence resonances in the NMR spectra indicates a preference for syndiotactic addition during the polymerization process [62]. However, this preference decreases with increasing extent of polymerization. Steric hindrance at the polymer growing site is probably responsible for the syndiotactic stereospecificity, and the increasingly random lactide addition is due to interplay of kinetically and thermodynamically controlled reactions. Changes in viscosity during the melt polymerization additionally influence the stereochemistry. The effect of transesterification on the stereosequence distribution should be related to increasing time and hence increasingly randomize with increasing polymerization time until the stereosequence distribution in the polymer becomes random. The limiting invariant stereosequence intensity in PLA near equilibrium shows that transesterification and racemization are not frequent enough to influence the stereosequence distribution under the polymerization conditions [64].

REFERENCES

1. M. H. Hutchinson, J. R. Dorgan, D. M. Knauss, S. B. Hait, *J. Polym. Environ.* **2006**, *14*, 119–124.
2. J. M. Zhang, H. Tsuji, I. Noda, Y. Ozaki, *J. Phys. Chem. B* **2004**, *108*, 11514–11520.

3. N. S. Oliveira, J. Oliveira, T. Gomes, A. Ferreira, J. Dorgan, I. M. Marrucho, *Fluid Phase Equilibr*. **2004**, *222*, 317–324.
4. K. L. G. Ho, A. L. Pometto, *J. Environ. Polym. Degrad.* **1999**, *7*, 93–100.
5. K. N. Turhan, F. Sahbaz, *Polym. Int*. **2001**, *50*, 1138–1142.
6. M. Mathlouthi, *Food Packaging and Preservation*, Blackie, **1994**, XVI + 275 pp.
7. R. Auras, B. Harte, S. Selke, *Macromol. Biosci.* **2004**, *4*, 835–864.
8. R. Auras, Ph.D. thesis, Michigan State University, East Lansing, MI, 2004, p. 268.
9. J. Lunt, D. W. Farrington, S. Davies, R. S. Blackburn, Poly (lactic acid) fibers, in: *Biodegradable and Sustainable Fibres*, Woodhead Publishing Ltd., 2005, Chapter 6.
10. C. F. L. Ciolacu, N. R. Choudhury, N. K. Dutta, *Polym. Degrad. Stabil.* **2006**, *91*, 875–885.
11. M. Edge, R. Wiles, N. S. Allen, W. A. McDonald, S. V. Mortlock, *Polym. Degrad. Stabil.* **1996**, *53*, 141–151.
12. J. Ramiro, J. I. Eguiazabal, J. Nazabal, *J. Appl. Polym. Sci.* **2002**, *86*, 2775–2780.
13. Y. M. Wang, B. Steinhoff, C. Brinkmann, I. Alig, *Polymer* **2008**, *49*, 1257–1265.
14. F. Sondheimer, D. A. Benefraim, R. Wolovsky, *J. Am. Chem. Soc.* **1961**, *83*, 1675–1681.
15. M. C. Gupta, V. G. Deshmukh, *Colloid Polym. Sci.* **1982**, *260*, 514–517.
16. Chugh. N. N., Lalla J. K., *Indian Drugs* **1990**, *27*, 516–522.
17. D. W. VanKrevelen, *Properties of Polymers*, 3rd edition, Elsevier Science B.V., Amsterdam, The Netherlands, **1997**.
18. T. Malmgren, J. Mays, M. Pyda, *J. Therm. Anal. Calorim.* **2006**, *83*, 35–40.
19. H. Tsuji, S. H. Hyon, Y. Ikada, *Macromolecules* **1991**, *24*, 5651–5656.
20. N. Yui, P. J. Dijkstra, J. Feijen, *Makromol. Chem.* **1990**, *191*, 481–488.
21. H. R. Kricheldorf, R. Dunsing, *Makromol. Chem.* **1986**, *187*, 1611–1625.
22. J. Kobayashi, T. Asahi, M. Ichiki, A. Oikawa, H. Suzuki, T. Watanabe, E. Fukada, Y. Shikinami, *J. Appl. Phys.* **1995**, *77*, 2957–2973.
23. H. W. Siesler, K. Holland-Moritz, *Infrared and Raman Spectroscopy of Polymers*, 1980, VIII + 389 pp.
24. R. Mehta, V. Kumar, H. Bhunia, S. N. Upadhyay, *J. Macromol. Sci. Polym. Res.* **2005**, *C45*, 325–349.
25. M. Matsusaki, A. Kishida, N. Stainton, C. W. G. Ansell, M. Akashi, *J. Appl. Polym. Sci.* **2001**, *82*, 2357–2364.
26. M. H. Gutierrez-Villarreal, M. G. Ulloa-Hinojosa, J. G. Gaona-Lozano, *J. Appl. Polym. Sci.* **2008**, *110*, 163–169.
27. W. H. Song, Z. Zheng, W. L. Tang, X. L. Wang, *Polymer* **2007**, *48*, 3658–3663.
28. M. T. Khorasani, H. Mirzadeh, S. Irani, *Radiat. Phys. Chem.* **2008**, *77*, 280–287.
29. Y. S. Kim, E. S. Gil, T. L. Lowe, *Macromolecules* **2006**, *39*, 7805–7811.
30. Z. J. Ren, L. S. Dong, Y. M. Yang, *J. Appl. Polym. Sci.* **2006**, *101*, 1583–1590.
31. B. Braun, J. R. Dorgan, S. F. Dec, *Macromolecules* **2006**, *39*, 9302–9310.
32. P. Degee, P. Dubois, S. Jacobsen, H. G. Fritz, R. Jerome, *J. Polym. Sci. Polym. Chem.* **1999**, *37*, 2413–2420.
33. M. Jalabert, C. Fraschini, R. E. Prud'Homme, *J. Polym. Sci. Polym. Chem.* **2007**, *45*, 1944–1955.
34. G. Kister, G. Cassanas, M. Vert, *Polymer* **1998**, *39*, 267–273.
35. G. Kister, G. Cassanas, M. Vert, B. Pauvert, A. Terol, *J. Raman Spectrosc.* **1995**, *26*, 307–311.
36. C. M. B. Gonçalves, J. A. P. Coutinho, I. M. Marrucho, *Polymer*, submitted. Q2
37. D. Garlotta, *J. Polym. Environ.* **2001**, *9*, 63–84.
38. N. T. Paragkumar, E. Dellacherie, J. L. Six, *Appl. Surf. Sci.* **2006**, *253*, 2758–2764.
39. C. M. Johnson, A. B. Sugiharto, S. Roke, *Chem. Phys. Lett.* **2007**, *449*, 191–195.
40. A. B. Sugiharto, C. M. Johnson, H. B. De Aguiar, L. Alloatti, S. Roke, *Appl. Phys. Part B* **2008**, *91*, 315–318.
41. C. Aleman, B. Lotz, J. Puiggali, *Macromolecules* **2001**, *34*, 4795–4801.
42. S. Sasaki, T. Asakura, *Macromolecules* **2003**, *36*, 83858390.
43. K. Aou, S. L. Hsu, *Macromolecules* **2006**, *39*, 3337–3344.
44. S. H. Kang, S. L. Hsu, H. D. Stidham, P. B. Smith, M. A. Leugers, X. Z. Yang, *Macromolecules* **2001**, *34*, 4542–4548.
45. A. B. Sugiharto, C. M. Johnson, I. E. Dunlop, S. Roke, *J. Phys. Chem. C* **2008**, *112*, 7531–7534.
46. E. Meaurio, E. Zuza, N. Lopez-Rodriguez, J. R. Sarasua, *J. Phys. Chem. B* **2006**, *110*, 5790–5800.
47. J. R. Sarasua, N. L. Rodriguez, A. L. Arraiza, E. Meaurio, *Macromolecules* **2005**, *38*, 8362–8371.
48. J. M. Zhang, H. Sato, H. Tsuji, I. Noda, Y. Ozaki, *Macromolecules* **2005**, *38*, 1822–1828.
49. J. M. Zhang, H. Tsuji, I. Noda, Y. Ozaki, *Macromolecules* **2004**, *37*, 6433–6439.
50. P. Pan, W. Kai, B. Zhu, T. Dong, Y. Inoue, *Macromolecules* **2007**, *40*, 6898–6905.
51. J. M. Zhang, Y. X. Duan, H. Sato, H. Tsuji, I. Noda, S. Yan, Y. Ozaki, *Macromolecules* **2005**, *38*, 8012–8021.
52. P. J. Pan, B. Zhu, W. H. Kai, T. Dong, Y. Inoue, *Macromolecules* **2008**, *41*, 4296–4304.
53. H. Bourque, I. Laurin, M. Pezolet, J. M. Klass, R. B. Lennox, G. R. Brown, *Langmuir* **2001**, *17*, 5842–5849.
54. M. Tanaka, R. J. Young, *Biomacromolecules* **2006**, *7*, 2575–2582.
55. P. B. Smith, A. Leugers, S. H. Kang, X. Z. Yang, S. L. Hsu, *Macromol. Symp.* **2001**, *175*, 81–94.
56. *Characterization of Solid Polymers New Techniques and Developments*, 1994, XII + 368 pp.
57. K. A. M. Thakur, R. T. Kean, E. S. Hall, M. A. Doscotch, E. J. Munson, *Anal. Chem.* **1997**, *69*, 4303–4309.
58. J. E. Kasperczyk, *Macromolecules* **1995**, *28*, 3937–3939.

59. H. R. Kricheldorf, C. Boettcher, K. U. Tonnes, *Polymer* **1992**, *33*, 2817–2824.

60. H. R. Kricheldorf, I. Kreisersaunders, C. Boettcher, *Polymer* **1995**, *36*, 1253–1259.

61. M. T. Zell, B. E. Padden, A. J. Paterick, K. A. M. Thakur, R. T. Kean, M. A. Hillmyer, E. J. Munson, *Macromolecules* **2002**, *35*, 7700–7707.

62. K. A. M. Thakur, R. T. Kean, E. S. Hall, J. J. Kolstad, T. A. Lindgren, M. A. Doscotch, J. I. Siepmann, E. J. Munson, *Macromolecules* **1997**, *30*, 2422–2428.

63. A. Schindler, D. Harper, *J. Polym. Sci. Part C* **1976**, *14*, 729–734.

64. K. A. M. Thakur, R. T. Kean, E. S. Hall, J. J. Kolstad, E. J. Munson, *Macromolecules* **1998**, *31*, 1487–1494.

Author Query

1. Please check the inserted citation of Table 8.2 for correctness.
2. Please update Ref. 36.
3. Please provide y-axis in Figures 8.4 and 8.5.
4. Figure 8.7 is to be printed in black and white. Please amend the caption accordingly.